

# SAPL: Semantic-Agnostic Prompt Learning in CLIP for Weakly Supervised Image Manipulation Localization

Xinghao Wang

University of Science and Technology of China

Changtao Miao

University of Science and Technology of China

Dianmo Sheng

University of Science and Technology of China

Tao Gong

University of Science and Technology of China

Qi Chu

University of Science and Technology of China

Nenghai Yu

University of Science and Technology of China

Quanchen Zou

University of Science and Technology of China

Deyue Zhang

University of Science and Technology of China

Xiangzheng Zhang

University of Science and Technology of China

## Abstract

Malicious image manipulation threatens public safety and requires efficient localization methods. Existing approaches depend on costly pixel-level annotations which make training expensive. Existing weakly supervised methods rely only on image-level binary labels and focus on global classification, often overlooking local edge cues that are critical for precise localization. We observe that feature variations at manipulated boundaries are substantially larger than in interior regions. To address this gap, we propose Semantic-Agnostic Prompt Learning (SAPL) in CLIP, which learns text prompts that intentionally encode non-semantic, boundary-centric cues so that CLIP’s multimodal similarity highlights manipulation edges rather than high-level object semantics. SAPL combines two complementary modules Edge-aware Contextual Prompt Learning (ECPL) and Hierarchical Edge Contrastive Learning (HECL) to exploit edge information in both textual and visual spaces. The proposed ECPL leverages edge-enhanced image features to generate learnable textual prompts via an attention mechanism, embedding semantic-irrelevant information into text features, to guide CLIP focusing on manipulation edges. The proposed HECL extract genuine and manipulated edge patches, and utilize contrastive learning to boost the dis-

crimination between genuine edge patches and manipulated edge patches. Finally, we predict the manipulated regions from the similarity map after processing. Extensive experiments on multiple public benchmarks demonstrate that SAPL significantly outperforms existing approaches, achieving state-of-the-art localization performance.

## 1. Introduction

Digital images pervade modern information dissemination. Malicious image manipulations that spread fabricated news, enable academic fraud and support illicit activities pose significant threats to societal security. As a result, accurate detection and precise localization of manipulated regions has emerged as a critical research challenge.

Early techniques combined pixel-level cues including noise features boundary information and color inconsistencies to identify manipulated regions. In recent years fully supervised methods[3, 12, 22, 28] have dominated. CAT-Net[15] learns manipulation artifacts in both RGB and DCT domains. MVSS-Net[6] uses multi scale noise and boundary features for precise localization. Mantra-Net[35] employs fine-grained classification and boundary attention to precisely delineate manipulated edges. PROMPT-IML[17] aligns and fuses semantic and high-frequency features

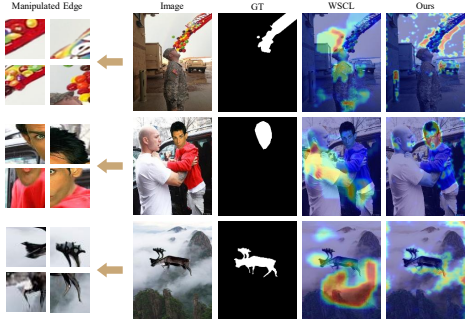


Figure 1. Subtle manipulation artifacts can be observed along the boundaries of manipulated regions. Our approach produces sharper heatmaps around manipulation boundaries.

from pre-trained vision models for cross-dataset generalization. Sparse-ViT[29] utilizes sparse self-attention to extract non-semantic cues, reducing parameter count while enhancing robustness. Re-MTKD[37] presents a multi teacher knowledge distillation framework that embeds both shared and unique manipulation patterns in the student model. Despite strong performance on training sets, these methods often suffer from poor generalization to unseen manipulation types, and the high cost of pixel-level annotations hinders large-scale dataset construction. In contrast, weakly supervised methods[43] rely solely on image-level binary labels, obviating the need for pixel masks while retaining localization accuracy and generalization capability. Compared to unsupervised[39] or semi-supervised schemes, weak supervision offers more stable optimization and requires more readily available annotations. For instance, WSCL[1, 24, 38] achieves localization through multi-noise view branches and cross-patch self-consistency. SO-WSL[44] refines pseudo-labels via iterative optimization. M<sup>2</sup>RL-Net[16] combines patch-level self-consistency and feature-level contrastive learning across multiple noise branches. Despite achieving significant results, these approaches often fail to systematically integrate edge information, which is essential for precise localization.

As established in image manipulation analysis[2, 23, 33, 35, 44], common manipulation types such as splicing[5], copy-move[26], and inpainting disrupt the local consistency of natural images. Interior regions usually preserve intrinsic cues such as CFA artifacts and JPEG traces, while manipulation boundaries act as interfaces between distinct image segments. This discontinuity results in variations of noise distribution, illumination, and texture gradients. Consequently, edges become the most reliable indicators of manipulation traces. To verify the importance of edge features, we conduct a statistical analysis of manipulation trace distributions as shown in Fig.2. Specifically, we compute the mean local variance of grayscale values, mean gradient magnitude (Sobel), intensity skewness, and excess kurtosis in four regions: manipulated edges, authentic edges, manipulated interiors, and authentic interiors. These met-

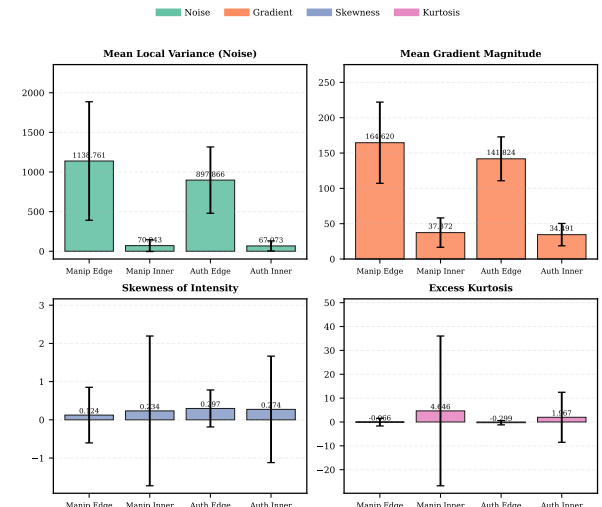


Figure 2. Four low-level statistics (mean local variance, mean gradient magnitude, intensity skewness and excess kurtosis) computed over four region types (manipulated edge / manipulated inner / authentic edge / authentic inner) on CASIAv2. Manipulated edges consistently show higher noise and gradient and altered higher-order statistics (mean  $\pm$  std), supporting the motivation to focus on boundary cues.

rics respectively capture the local noise fluctuation, structural strength, and higher-order statistical characteristics of each region. The results show that manipulated edges exhibit much stronger brightness variations than authentic edges, substantially higher gradient magnitudes, and noticeably altered skewness and kurtosis distributions, while the interior regions of both manipulated and authentic areas share similar local statistics. Existing weakly supervised methods[16, 38, 44] often overlook low level cues such as edge and noise patterns, which limits their ability to learn boundary discriminative features without pixel level supervision. Although CLIP[25] is powerful for semantic alignment, it is even less sensitive to these low level signals. This observation motivates us to exploit edge information as a fundamental structural signal that directly reflects inconsistencies caused by manipulation. However, effectively utilizing edge information under weak supervision is highly challenging because pixel level annotations are unavailable to explicitly guide boundary learning.

To address this issue, we introduce Semantic-Agnostic Prompt Learning (SAPL), a weakly-supervised framework that explicitly learns semantic-agnostic text prompts to inject boundary-centric cues into CLIP[25], thereby steering multimodal alignment away from object semantics toward manipulation artifacts. Specifically, we propose an Edge-aware Contextual Prompt Learning module (ECPL) built on CLIP[25]. ECPL constructs learnable prompt templates for the real and manipulated class and personalizes these prompts by embedding per image edge cues derived from patch level features and edge maps. This strategy compels

the model to attend to non semantic boundary discrepancies thereby enhancing localization precision and cross dataset generalization without reliance on pixel-level masks. To further strengthen feature discrimination, we introduce a Hierarchical Edge Contrastive Learning module (HECL). HECL assumes that edge features of the same class should cluster closely in the latent space. It selects high confidence edge patches across multiple encoder layers forms positive and negative pairs based on edge cues and applies contrastive learning to enforce separation between authentic and manipulated boundaries. The combination of ECPL and HECL enables SAPL to efficiently exploit edge information within CLIP[25], achieving precise and robust image manipulation localization under weak supervision.

Experiments show that our method achieves state-of-the-art performance in both manipulation detection and localization. Our main contributions are as follows:

- We design Edge-aware Contextual Prompt Learning, which embeds image-specific edge cues into learnable prompts for authentic and manipulated classes, guiding model to attend to non-semantic boundary discrepancies
- We design Hierarchical Edge Contrastive Learning that selects confident edge patches from multiple encoder layers and applies contrastive objectives to sharpen the separation between authentic and manipulated boundaries.
- We present SAPL, a weakly supervised framework that requires no pixel-level annotations and achieves state-of-the-art performance on multiple benchmarks for manipulation detection and localization.

## 2. Related Work

### 2.1. Weakly Supervised Image Manipulation Localization

Traditional unsupervised methods detect manipulations by extracting low-level features such as CFA artifacts and double JPEG traces[8, 21]. While annotation-free, they rely on strong assumptions that limit generalization to diverse manipulations. Fully supervised approaches[4, 13, 14, 31, 32, 36, 42] achieve high accuracy using pixel-level labels but incur significant annotation costs. Weakly supervised methods, that requiring only image-level labels have gained attention because they can produce fine-grained predictions with minimal supervision. Representative works include WSCL[38] which leverages multi-view noise branches and cross-patch consistency. SO-WSL[44] refines pseudo-labels through iterative optimization. WSCCL[2] adopts a cross contrastive learning strategy under image-level supervision to improve localization performance. M<sup>2</sup>RL-Net[16] introduces contrastive learning on top of multi-noise representations. Edge-based approaches have also shown promise. For example EdgeCAM[23] leverages manipulating edge-based class activation maps to refine weakly

supervised localization. Compared to existing methods, our approach deeply leverages edge cues in both textual and visual representations, achieving significant improvements in image-level alignment and pixel-level discrimination, thereby enabling more robust and fine-grained localization of various manipulation traces.

### 2.2. Contrastive Language and Image Pretraining

Contrastive Language and Image Pretraining (CLIP)[25] is a cross-modal pretraining model that learns a unified semantic space via contrastive learning on large-scale image-text pairs. It has shown strong performance in zero-shot classification, image-text retrieval, and open-world recognition. Recent efforts have adapted CLIP to downstream vision tasks. CoOp[40] and CoCoOp[41] replace hand-crafted templates with learnable prompts to better align with downstream category features. DenseCLIP[27] extends CLIP[25] to pixel-level tasks by generating dense activation maps for weakly supervised semantic segmentation. Other works introduce fusion mechanisms to integrate CLIP’s[25] language priors with visual features for object detection and anomaly detection. While CLIP[25] excels at semantic-level generalization, its sensitivity to low-level structural details and image perturbations is limited. Since manipulation traces rely more on edge cues, local textures, and subtle disturbances rather than high-level semantics, our core objective is to enhance CLIP’s[25] ability to perceive and discriminate manipulation cues without sacrificing its cross-modal modeling strengths.

## 3. Methodology

### 3.1. Overview of SAPL

We propose Semantic-Agnostic Prompt Learning (SAPL), as illustrated in Fig.3, which consists of two core components: Edge-aware Contextual Prompt Learning (ECPL) and Hierarchical Edge Contrastive Learning (HECL). Under weak supervision, SAPL uses only image-level binary labels without pixel annotations. During training, the input image is processed by the CLIP image encoder to extract multi-layer patch features, while an adaptive soft edge generator produces a soft edge map. ECPL utilizes this edge map to generate edge-aware, semantic-agnostic prompts,  $T_{HECL}$ , which are concatenated with the REAL/FAKE prompts  $T_R$  and  $T_F$ , and then passed through the frozen text encoder to obtain corresponding text features. This process enables CLIP[25] to emphasize manipulation-induced inconsistencies during image-text similarity computation instead of relying on high-level semantics. HECL selects high-confidence edge patches from the patch features  $f_{patch_i}$  of the selected layers, and employs dual queues with contrastive loss to reinforce edge representations. The overall loss combines the classification loss with a linearly

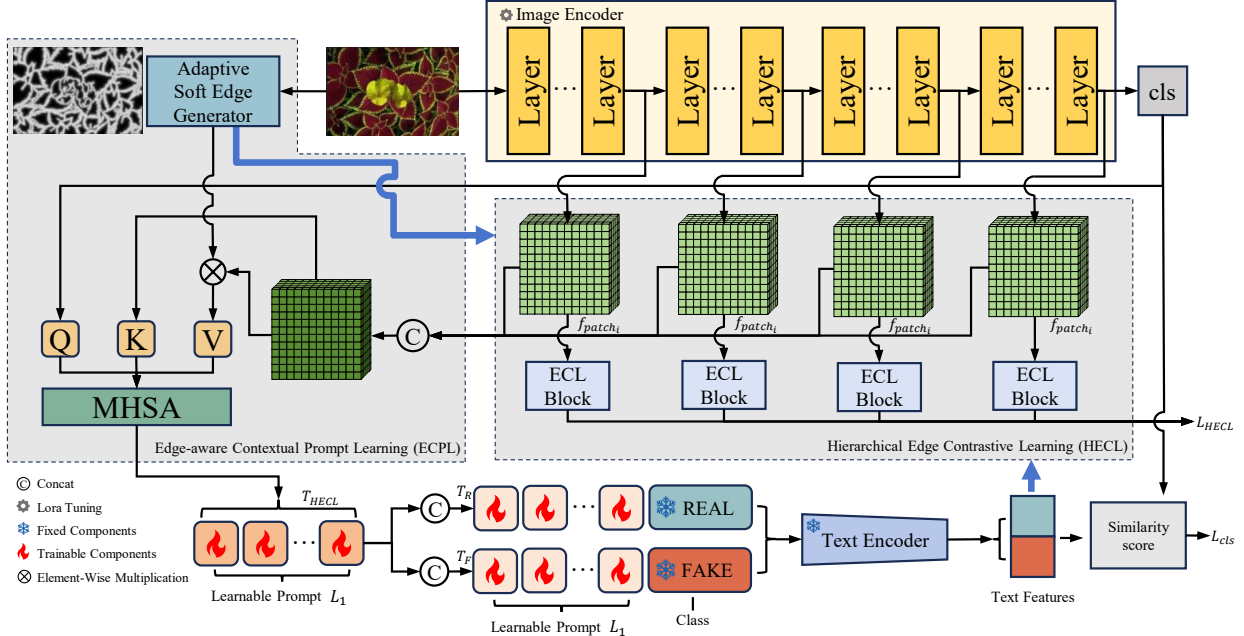


Figure 3. The SABL architecture. SABL implements semantic-agnostic prompt learning via two complementary modules: Edge-aware Contextual Prompt Learning (ECPL) and Hierarchical Edge Contrastive Learning (HECL). During training, SABL extracts patch features and soft edge maps, applies ECPL for prompt generation and HECL for edge contrastive learning, and optimizes classification plus contrastive losses. At inference, it uses patch–text similarity to produce localization maps and decide the class.

weighted HECL loss. During inference, SABL computes multi-layer patch–text similarity maps and aggregates them to produce localization results, while the final image-level classification is determined by the text prompt with the highest similarity score.

### 3.2. Edge-aware Contextual Prompt Learning

In conventional CLIP-based frameworks, manually crafted text prompts primarily emphasize high-level semantic information of depicted objects. However, precise manipulation localization relies on subtle low-level irregularities and diverse manipulation traces rather than semantic content. Due to the high variability of manipulation patterns, a single global prompt cannot capture all boundary anomalies. To address this, we introduce learnable text prompts that automatically adapt to diverse manipulation characteristics. Furthermore we inject edge features into the prompt generation process to steer the model’s attention toward boundary irregularities rather than high-level semantics. This Edge-aware Contextual Prompt Learning (ECPL) module unites the flexibility of learnable prompts with the discriminative power of edge cues, forming a data-driven mechanism that highlights a wide range of manipulation patterns. The following sections detail the implementation of this module.

Conventional binary edge maps contain too sparse information and lack hierarchical detail, causing the network to fail to converge and preventing it from capturing the subtle perturbations critical for manipulation localization. To address this, we propose an Adaptive Soft Edge Genera-

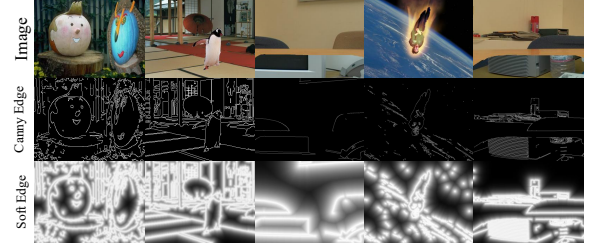


Figure 4. Canny-based Adaptive Soft Edge Map.

tor. First we apply the Canny operator to extract initial edges from the input image. Next we perform a distance transform on non-edge regions to compute the Euclidean distance from each pixel to its nearest edge. We then dynamically compute an exponential decay factor  $k$  based on the proportion of edge pixels and apply it to the distance map. As a result, pixels near boundaries receive weights close to one, while those farther away decay rapidly toward zero, producing a soft edge map that smoothly attenuates outward from the boundaries (see Fig.4). This soft map preserves precise boundary localization and introduces continuous multi-scale weight variations within neighborhoods, providing rich edge features for subsequent prompt generation. The generation process is formalized as:

$$E_{\text{soft}}(x, y) = \exp \left( -k \cdot \min_{(i, j) \in C(I)} \|(x - i, y - j)\|_2 \right) \quad (1)$$

where  $k$  is an adaptive coefficient dynamically adjusted according to edge density,  $I$  represents the input image, and

$C(I)$  represents the initial edge set obtained by the Canny operator.

Although the original CLIP[25] pre-trained model excels at capturing semantic concepts, it lacks sensitivity to subtle manipulation artifacts and thus is inadequate for manipulation localization. To enhance adaptability to diverse manipulation patterns, we introduce learnable global text prompts, as defined in Eq.(2). These prompts embed various manipulation characteristics into the textual embedding space, thereby amplifying anomalous signals originating from manipulated regions during multimodal alignment and enabling precise detection and discrimination of non-semantic details.

$$\begin{aligned} T_R &= [R_1][R_2] \dots [Real][Image] \\ T_F &= [F_1][F_2] \dots [Fake][Image] \end{aligned} \quad (2)$$

However, a single global prompt cannot capture the rich and varied edge characteristics in each image. Since nearly all manipulations introduce discontinuities or artifacts at object boundaries, we integrate the adaptive soft edge map with multi-layer patch features and employ a multi-head self-attention (MHSA) mechanism to generate edge-aware text prompts as formulated in Eq.(3). In this process, soft edge features guide the attention computation alongside patch features, enabling the resulting text embeddings to preserve the generalizability of learnable prompts while precisely focusing on boundary anomalies in each image.

$$\begin{aligned} Q &= f_{cls}, \quad K = P \left( \sum_i f_{patch_i} \right), \\ V &= P \left( \sum_i f_{patch_i} \right) \circ E_{soft}(x, y), \\ T_{ECPL} &= \text{MHSA}(Q, K, V) \end{aligned} \quad (3)$$

where  $f_{cls}$  denotes the CLS feature extracted by the image encoder,  $f_{patch_i}$  indicates the patch features from the  $i$ -th layer,  $P(\cdot)$  is the projection function,  $E_{soft}(x, y)$  denotes the soft edge map value at  $(x, y)$ ,  $\circ$  denotes element-wise multiplication, and MHSA refers to multi-head self-attention.

This design enables prompt templates to capture non-semantic manipulation cues while maintaining generalizability and adapting to image-specific boundary variations, thereby effectively facilitating the localization of manipulated regions across diverse manipulation types.

### 3.3. Hierarchical Edge Contrastive Learning

In the weakly supervised setting, the model relies solely on image-level labels and often struggles to distinguish manipulated regions from authentic content. This challenge becomes more severe when manipulated areas are small, have blurred boundaries, or share semantic similarity with surrounding regions. While the ECPL module enhances manipulation cues via edge guidance in the text embedding space, it alone cannot fully capture latent manipulation patterns within the image feature domain. To further

leverage CLIP’s[25] strong unified image-text modeling capabilities, we propose the Hierarchical Edge Contrastive Learning (HECL) module. HECL explores local representation patterns of manipulated images at the patch level. The core insight is that manipulation often introduces subtle and structured perturbations in localized regions, which are particularly prominent along edges. By employing contrastive learning to enforce consistent representations for manipulated edge regions, HECL significantly improves the model’s ability to discriminate between manipulated and authentic content.

Specifically, at the selected feature layer, the HECL module constructs a similarity map between image patch features and learnable text prompt features, then weights it with the soft edge map to enhance the separability of manipulated and authentic edges in the image domain. Based on the weighted similarity response, we select the top  $K$  pixel locations with the highest confidence scores from both manipulated and authentic edge regions, and extract their corresponding patch features, denoted as  $\{f_e^+\}^K$  and  $\{f_e^-\}^K$ , respectively. These edge-aligned features are then projected into a unified embedding space via the projection head  $P(\cdot)$  and used as positive and negative samples for contrastive learning:

$$\begin{aligned} \{f_e^+\}^K &= \{\{sim\{f_{patch_i}, t^+\} \circ E_{soft}(x, y)\} \circ f_{patch_i}\}^K, \\ \{f_e^-\}^K &= \{\{sim\{f_{patch_i}, t^-\} \circ E_{soft}(x, y)\} \circ f_{patch_i}\}^K, \\ z_i^+ &= P(\{f_e^+\}^K) \quad z_i^- = P(\{f_e^-\}^K) \end{aligned} \quad (4)$$

where  $\{f_e^+\}^K$  and  $\{f_e^-\}^K$  denote the sets of the top  $K$  weighted patch features for manipulated-edge positives and authentic-edge negatives,  $i$  denotes the selected feature layer,  $f_{patch_i}$  indicates the patch features extracted from the  $i$ -th layer,  $t^+$  and  $t^-$  represent the learnable text prompt features for manipulated and authentic classes,  $z_i^\pm$  denote the positive and negative sample features at the  $i$ -th layer,  $sim\{f_{patch_i}, t^\pm\}$  computes the similarity score between patch feature and its corresponding text prompt feature,  $P(\cdot)$  represents the projection function,  $\circ$  denotes element-wise multiplication, and  $E_{soft}(x, y)$  denotes the soft edge map value at  $(x, y)$ .

To prevent localized perturbations in a single image from dominating contrastive learning, HECL employs dual queues for positive and negative samples. Each queue dynamically stores feature vectors extracted from recent training batches, forming a temporally updated memory bank instead of a static sample pool. This design significantly improves sample diversity and training stability, while mitigating gradient fluctuations caused by small batch variations through cross-batch enrichment. Under the weak supervision setting, where pixel-level labels are unavailable and category ambiguity may occur, the queue mechanism further reduces the adverse impact of mis-sampled instances on the model. Specifically, newly extracted positive and

Table 1. Comparison of Image Manipulation Detection and Localization Methods across Multiple Datasets. Best and second-best weakly supervised results are in **bold** and underline, respectively. Un.: unsupervised; Full.: fully supervised; Weak.: weakly supervised. Note: NIST16 contains only manipulated images.

	Method	Source	CASIAv1		Columbia		COVERAGE		IMD2020		NIST16		Average		
			I-AUC	P-F1	I-AUC	P-F1	I-AUC	P-F1	P-F1	I-AUC	P-F1	I-AUC	P-F1	I-AUC	P-F1
Un.	NOII[21]	<i>IVC09</i>	0.500	0.157	0.500	0.311	0.500	0.205	0.500	0.124	0.089	0.500	0.190		
	CFAI[8]	<i>TIFS12</i>	0.482	0.140	0.344	0.320	0.525	0.188	0.500	0.111	0.106	0.500	0.188		
Full.	Mantra-Net[35]	<i>CVPR19</i>	0.141	0.155	0.701	0.364	0.490	0.286	0.719	0.122	0.000	0.513	0.185		
	CAT-Net[15]	<i>WACV21</i>	0.630	0.276	0.782	0.352	0.572	0.134	0.721	0.102	0.138	0.693	0.200		
	MVSS-Net[35]	<i>TPAMI22</i>	0.937	0.452	0.980	0.638	0.731	0.453	0.656	0.260	0.292	0.826	0.419		
	GSR-Net[12]	<i>AAAI20</i>	0.502	0.387	0.502	0.613	0.515	0.285	0.505	0.175	0.283	0.506	0.349		
	RRU-Net[3]	<i>CVPR19</i>	0.507	0.225	0.497	0.452	0.495	0.189	0.512	0.232	0.265	0.503	0.273		
	FCN+DA	<i>ICCV21</i>	0.796	0.441	0.762	0.223	0.541	0.199	0.746	0.270	0.160	0.711	0.260		
Weak.	MIL-FCN[24]	<i>ICLR15</i>	0.647	0.117	0.807	0.089	0.542	0.121	0.578	0.097	0.024	0.644	0.090		
	MIL-FCN+WSCL[38]	<i>ICCV23</i>	0.829	0.172	0.920	0.270	0.584	0.178	0.733	0.193	0.110	0.766	0.185		
	Araslanov[1]	<i>CVPR20</i>	0.642	0.112	0.773	0.102	0.560	0.127	0.665	0.094	0.026	0.660	0.092		
	Araslanov+WSCL[38]	<i>ICCV23</i>	0.796	0.153	0.917	0.362	0.591	0.201	0.701	0.173	0.099	0.751	0.198		
	M <sup>2</sup> RL-Net[16]	<i>AAAI25</i>	<b>0.948</b>	<u>0.347</u>	<b>0.999</b>	<b>0.434</b>	<u>0.716</u>	0.213	<u>0.827</u>	0.248	0.113	<u>0.862</u>	0.265		
	SO-WSL[44]	<i>ICASSP25</i>	0.881	0.334	<u>0.942</u>	0.385	0.702	<u>0.239</u>	0.556	<u>0.259</u>	<b>0.288</b>	0.770	<u>0.301</u>		
	Ours	-	0.931	<b>0.356</b>	<b>0.999</b>	<u>0.432</u>	<b>0.772</b>	<u>0.323</u>	<b>0.906</b>	<u>0.364</u>	<u>0.274</u>	<b>0.902</b>	<b>0.349</b>		

Table 2. Ablation Study of **ECPL** and **HECL** Modules. “-” denotes no module applied. The baseline applies only LoRA tuning on the CLIP image encoder.

ECPL	HECL	CASIAv1		IMD2020		Avg	
		I-AUC	P-F1	I-AUC	P-F1	I-AUC	P-F1
-	-	0.887	0.175	0.854	0.220	0.871	0.198
✓	-	0.924	0.320	0.897	0.289	0.911	0.305
-	✓	0.921	0.331	0.895	0.372	0.908	0.352
✓	✓	0.931	<b>0.356</b>	0.906	0.364	<b>0.919</b>	<b>0.360</b>

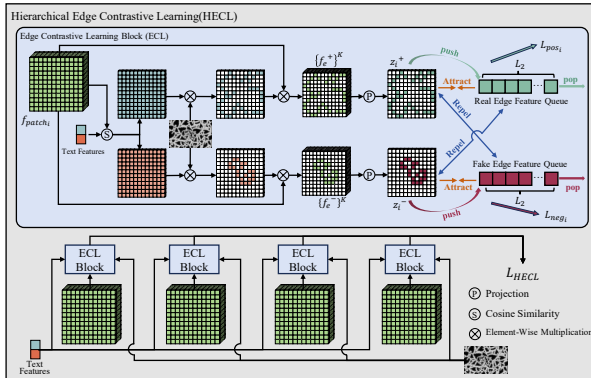


Figure 5. Hierarchical Edge Contrastive Learning. The ECL block computes similarity maps between patch features and text features, then uses the soft edge map to select the high-confidence patches for contrastive learning.

negative samples are enqueued in sequence, while the oldest entries are dequeued, ensuring that the queue maintains both recent dynamic features and sufficient historical context. In addition, HECL adopts a hierarchical structure that performs edge-aware contrastive learning across multiple feature depths, enabling progressive refinement from coarse to fine edge representations. We define the positive sample

and the negative sample contrastive learning loss as:

$$\mathcal{L}_{\text{pos}_i} = -\log \frac{\exp(\frac{\text{sim}(z_i^+, p_i)}{\tau})}{\exp(\frac{\text{sim}(z_i^+, p_i)}{\tau}) + \sum_{j=1}^{L_2} \exp(\frac{\text{sim}(z_i^+, n_j)}{\tau})} \quad (5)$$

$$\mathcal{L}_{\text{neg}_i} = -\log \frac{\exp(\frac{\text{sim}(z_i^-, n_i)}{\tau})}{\exp(\frac{\text{sim}(z_i^-, n_i)}{\tau}) + \sum_{j=1}^{L_2} \exp(\frac{\text{sim}(z_i^-, p_j)}{\tau})} \quad (6)$$

where  $\mathcal{L}_{\text{pos}_i}$  and  $\mathcal{L}_{\text{neg}_i}$  denote the contrastive losses for the positive and negative samples at the  $i$ -th layer,  $z_i^{\pm}$  denote the positive and negative sample features at the  $i$ -th layer, the positive key  $p_i$  is selected as the prototype in  $queue_{\text{pos}}$  with the highest cosine similarity to  $z_i^+$ , the negative key  $n_i$  is selected as the prototype in  $queue_{\text{neg}}$  with the highest cosine similarity to  $z_i^-$ ,  $p_j$  for  $j = 1, \dots, L_2$  are all positive keys stored in  $queue_{\text{pos}}$ ,  $n_j$  for  $j = 1, \dots, L_2$  are all negative keys stored in  $queue_{\text{neg}}$ ,  $\text{sim}(\cdot, \cdot)$  denotes the cosine similarity function, and  $\tau$  is the temperature parameter controlling the concentration of the distribution.

Overall, the HECL loss function can be expressed as Eq.(6).

$$\mathcal{L}_{\text{HECL}} = \frac{1}{N} \sum_{i=1}^N [\mathcal{L}_{\text{pos}_i} + \mathcal{L}_{\text{neg}_i}] \quad (6)$$

where  $N$  denotes the number of Edge Contrastive Learning (ECL) Blocks.

This hierarchical contrastive strategy captures large-scale boundary perturbations in lower-level features while focusing on fine-grained edge artifacts in higher-level features. It enables similar edge types to cluster naturally in the feature space while effectively increasing the representational distance between authentic and manipulated edges. When paired with ECPL’s edge-enhancement in the text domain, HECL delivers complementary contrastive supervision in the image domain. These two strategies work collaboratively to promote clearer separation of manipulated

regions across multimodal feature hierarchies, achieving more robust and detailed image manipulation localization under weak supervision.

### 3.4. Loss

As shown in Fig.3, our framework comprises two loss terms: the binary classification loss  $\mathcal{L}_{\text{cls}}$  and the Hierarchical Edge Contrastive Learning loss  $\mathcal{L}_{\text{HECL}}$ . For the binary classification loss, we employ the similarity metric from CLIP[25] and take the matching score between the image and the learnable text prompt as the classification criterion. To fully exploit the edge contrastive information extracted by the HECL module, we gradually increase the weight coefficient  $w(t)$  of the HECL loss according to a predefined linear schedule. This design enables the model to focus on fundamental semantic alignment during the early training stages and to emphasize precise distinction at the edge level in later stages. The overall loss function is defined as follows:

$$\mathcal{L}_{\text{all}} = \mathcal{L}_{\text{cls}} + w(t) \cdot \mathcal{L}_{\text{HECL}} \quad (7)$$

where  $w(t)$  denotes the weight of linear increase.

## 4. Experiments

### 4.1. Implementation Details

We train on CASIAv2 using only image-level binary labels without pixel annotations, evaluation is conducted on CASIAv1 [7] for intra-dataset testing, on Columbia [10], COVERAGE [34] and IMD2020 [23] for cross-dataset classification and localization, and on NIST16 [9] for localization only, reporting I-AUC for detection and P-F1 for pixel-level localization, consistent with prior work. We adopt the CLIP [25] ViT-L/14@336px backbone, freeze all parameters and fine-tune only only the LoRA [11] adapters of the image encoder, training on three NVIDIA RTX 3090 GPUs with PyTorch 2.0. Input images are resized so that the longer side is 512 px and padded to 512x512, optimized with AdamW [18] at a batch size of 12 and a learning rate of 1e-5 for 30 epochs. In ECPL, the learnable prompt length is set to 12, in HECL the positive and negative queue lengths are set to 1024, ECL blocks use layers 6, 12, 18 and 24, and the HECL loss weight  $w(t)$  increases linearly to 0.1.

### 4.2. Comprehensive Evaluation of SAPL

#### 4.2.1. State-of-the-Art Comparison

Tab.1 shows that under weak supervision our SAPL outperforms the prior weakly supervised detector by +4.6% in cross-dataset average I-AUC, and even surpasses the fully supervised MVSS-Net [6] by +9.2% , demonstrating stronger generalization and robustness. For localization, SAPL achieves a +3.9% gain in average P-F1 over the best weakly supervised method, reaching levels comparable to

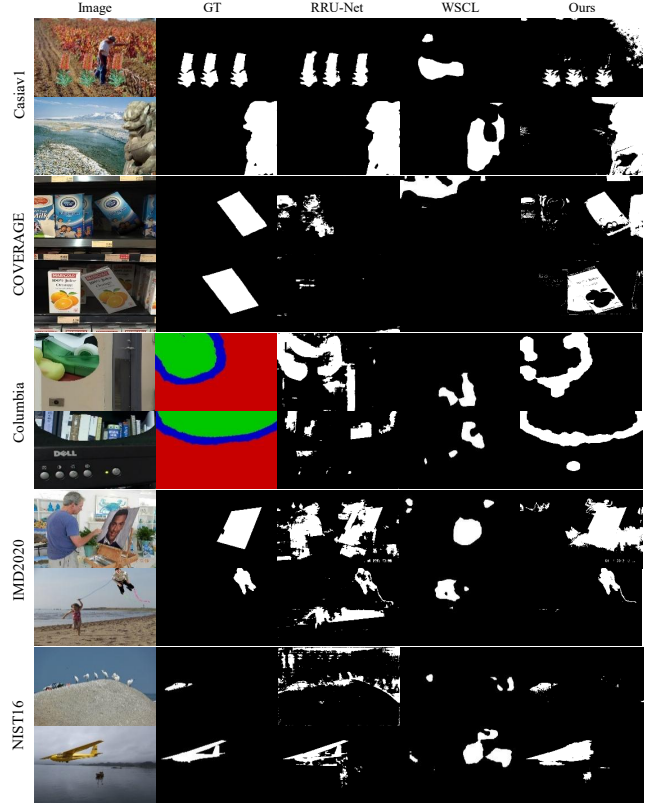


Figure 6. Qualitative Results on Five Datasets. From left to right: Image, GT, RRU-Net, WSCL, Ours

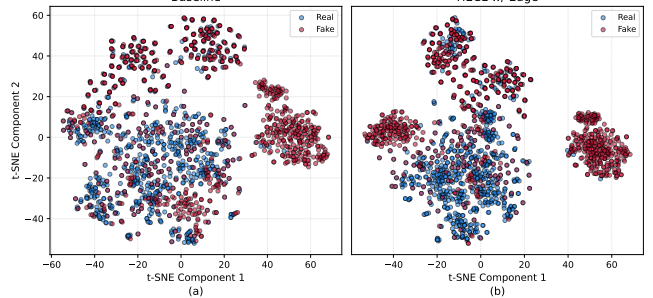


Figure 7. T-SNE Visualization of Embedding Spaces for w/o HECL and w/ HECL in the SAPL framework on CASIAv1, Demonstrating the HECL module's Significant Separation of Genuine and Manipulated Samples.

fully supervised models. These gains stem from our edge-guided modules, which effectively capture boundary artifacts without pixel-level masks.

#### 4.2.2. Visualization and Feature Analysis

Fig.6 presents visual comparisons with several open-source weakly supervised image manipulation localization methods. Our approach yields sharper boundaries and more accurate localization of manipulated regions. Furthermore, compared to representative fully supervised methods, it exhibits stronger generalization to unseen data, which under-

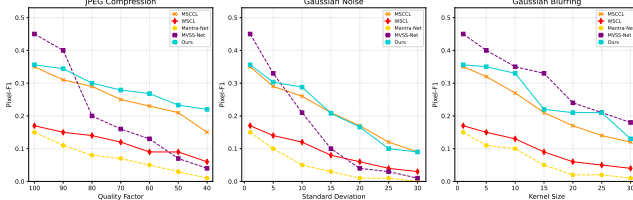


Figure 8. Robustness Evaluation of JPEG Compression, Gaussian Noise, and Gaussian Blurring on the CASIAv1 Dataset. Dashed lines represent fully supervised methods, and solid lines represent weakly supervised methods.

scores the effectiveness of weak supervision in complex scenarios.

To further analyze feature representation capability, we visualize the feature distributions of three model variants using t-SNE [20]: the baseline w/o HECL and HECL w/ edge information, as shown in Fig.7. The full HECL achieves a clearer separation between authentic and manipulated regions in the feature space, confirming its effectiveness in enhancing feature discriminability.

#### 4.2.3. Robustness Under Common Image Perturbations

To evaluate the model’s robustness against common real-world degradation scenarios, we follow standard protocols [16, 19, 38, 44] and conduct performance assessments on CASIAv1 [7] dataset under varying levels of JPEG compression [30], Gaussian blur and Gaussian noise. As shown in Fig.8, SAPL achieves more stable P-F1 scores compared to fully supervised baselines and consistently outperforms existing weakly supervised methods. These results confirm that our approach exhibits excellent robustness and generalization capability under diverse perturbation conditions.

### 4.3. Ablation Study

#### 4.3.1. Ablation Study on SAPL

Tab.2 presents the results of the ablation study evaluating the combined effect of the ECPL and HECL modules on the CASIAv1 [7] and IMD2020 [23] datasets. When ECPL is used independently, the average I-AUC increases by 4.6% and the average P-F1 improves by 54.0%. Using HECL alone leads to improvements of 4.2% in average I-AUC and 77.8% in average P-F1. When both modules are applied together, the model achieves an average I-AUC gain of 5.5% and an average P-F1 gain of 81.8%, achieving the best performance. These results confirm that under weak supervision, jointly leveraging edge cues from textual and visual features enables more accurate and efficient localization of manipulated regions.

#### 4.3.2. Ablation Study on ECPL Configuration Variants

We conduct ablation experiments to evaluate different ECPL configurations including CoOp style prompts, CoCoOp style prompts, and ECPL variants without and with

Table 3. Ablation study of **Edge-aware Contextual Prompt Learning (ECPL)** configuration variants w/ and w/o edge information. Baseline applies LoRA tuning on CLIP image encoder.

Methods	CASIAv1		IMD2020		Avg	
	I-AUC	P-F1	I-AUC	P-F1	I-AUC	P-F1
Baseline (Clip + LoRA)	0.887	0.175	0.854	0.220	0.871	0.198
Baseline + ECPL (w/o Edge)	0.904	0.271	0.868	0.257	0.886	0.264
Baseline + ECPL (w/ Edge)	0.924	0.320	0.897	0.289	<b>0.911</b>	<b>0.305</b>

Table 4. Comparison of different contextual prompt tuning strategies. CoOp and CoCoOp represent fixed and dynamic prompt tuning, respectively.

Methods	CASIAv1		IMD2020		Avg	
	I-AUC	P-F1	I-AUC	P-F1	I-AUC	P-F1
CoOp-style Prompt Tuning	0.893	0.165	0.862	0.190	0.878	0.178
CoCoOp-style Prompt Tuning	0.901	0.230	0.851	0.213	0.876	0.222
Baseline + HECL (w/ Edge)	0.924	0.320	0.897	0.289	<b>0.911</b>	<b>0.305</b>

edge information. Tab.3 reports ECPL performance on the CASIAv1[7] and IMD2020[23] datasets in terms of detection measured by average I-AUC and localization measured by average P-F1. The results show that ECPL yields notable gains even without edge information. When edge features are further mapped into the text space ECPL more accurately describes manipulated boundaries. This improves feature discriminability and tightens alignment between predicted and ground truth boundaries. Compared with the baseline the average I-AUC and average P-F1 increase by 4.6% and 54.0% respectively which confirms the central role of edge enhanced patch features in weakly supervised manipulation detection and localization.

Tab.4 compares CoOp style prompts, CoCoOp style prompts and our method. CoOp uses no image information and CoCoOp uses only the class token. By integrating edge cues and the full set of image features our method further improves performance. In this setting the average I-AUC and average P-F1 increase by 3.7% and 71.3% respectively over the CoOp and CoCoOp variants.

#### 4.3.3. Ablation Study on HECL Configuration Variants

We further evaluate HECL variants without and with edge information. As shown in Tab.5, compared to the baseline that only applies LoRA tuning to the image encoder, introducing HECL without edge information alone yields a 2.2% improvement in average I-AUC and a 38.8% improvement in average P-F1. When edge information is incorporated into HECL, the average I-AUC and average P-F1 are further increased to 4.2% and 77.8%, respectively. These results demonstrate that in weakly supervised image manipulate detection and localization tasks, HECL effectively enhances hierarchical feature edge modeling, leading to more accurate localization of manipulated regions.

#### 4.3.4. Ablation Study on Hyperparameter

We further examine the influence of two key hyperparameters on model performance: the length  $L_1$  of the learnable text prompt in the ECPL module and the queue length  $L_2$  used for contrastive learning. As shown in Tab.6, in-

Table 5. Ablation study of **Hierarchical Edge Contrastive Learning (HECL)** configuration variants w/ and w/o edge information. Baseline applies LoRA tuning on CLIP image encoder.

Methods	CASIAv1		IMD2020		Avg	
	I-AUC	P-F1	I-AUC	P-F1	I-AUC	P-F1
Baseline (Clip + LoRA)	0.887	0.175	0.854	0.220	0.871	0.198
Baseline + HECL (w/o Edge)	0.907	0.227	0.874	0.323	0.891	0.275
Baseline + HECL (w/ Edge)	0.921	0.331	0.895	0.372	<b>0.908</b>	<b>0.352</b>

Table 6. Ablation study of Learnable Prompt Length ( $L_1$ ) and Contrastive Learning Queue Length ( $L_2$ ) on CASIAv1 (P-F1)

$L_1$	256	512	1024	2048	4096
8	0.238	0.289	0.320	0.323	0.335
12	0.242	0.328	<b>0.356</b>	0.360	0.362
16	0.241	0.332	0.349	0.359	0.360
20	0.223	0.330	0.354	0.358	0.352

creasing  $L_1$  leads to a significant performance improvement that gradually saturates. A larger  $L_2$  enhances the discrimination between positive and negative samples, resulting in higher P-F1 scores, but also incurs additional computational cost. To balance effectiveness and efficiency, we set  $L_1 = 12$  and  $L_2 = 1024$  as the default configuration.

## 5. Conclusion

We presented SAPL, a weakly-supervised framework that introduces semantic-agnostic prompt learning to adapt CLIP for image manipulation localization. By injecting boundary-centric signals into textual prompts (ECPL) and reinforcing edge representation separation in the visual domain (HECL), SAPL steers multimodal alignment away from object semantics and toward manipulation artifacts, achieving robust pixel-level localization under image-level supervision. However, our current framework is primarily designed for local manipulation scenarios and may not generalize well to global or full-image manipulations where boundary cues are absent. Moreover, frequency-domain artifacts and other non-spatial cues are not explicitly modeled, which could limit performance under certain post-processing operations. Future work will explore integrating frequency-domain representations and developing adaptive weak-label generation strategies to further enhance localization accuracy and robustness.

## References

- [1] Nikita Araslanov and Stefan Roth. Single-stage semantic segmentation from image labels. In *Proceedings of the IEEE/CVF conference on computer vision and pattern recognition*, pages 4253–4262, 2020. [2](#), [6](#)
- [2] Ruyi Bai. Weakly-supervised cross-contrastive learning network for image manipulation detection and localization. *Knowledge-Based Systems*, 310:113033, 2025. [2](#), [3](#)
- [3] Xiuli Bi, Yang Wei, Bin Xiao, and Weisheng Li. Rru-net: The ringed residual u-net for image splicing forgery detection. In *Proceedings of the IEEE Conference on Computer Vision and Pattern Recognition Workshops*, pages 0–0, 2019. [1](#), [6](#)
- [4] Xinru Chen, Chengbo Dong, Jiaqi Ji, Juan Cao, and Xirong Li. Image manipulation detection by multi-view multi-scale supervision. In *Proceedings of the IEEE/CVF international conference on computer vision*, pages 14185–14193, 2021. [3](#)
- [5] Davide Cozzolino, Giovanni Poggi, and Luisa Verdoliva. Splicebuster: A new blind image splicing detector. In *2015 IEEE International Workshop on Information Forensics and Security (WIFS)*, pages 1–6, 2015. [2](#)
- [6] Chengbo Dong, Xinru Chen, Ruohan Hu, Juan Cao, and Xirong Li. Mvss-net: Multi-view multi-scale supervised networks for image manipulation detection. *IEEE Transactions on Pattern Analysis and Machine Intelligence*, 45(3):3539–3553, 2022. [1](#), [7](#)
- [7] Jing Dong, Wei Wang, and Tieniu Tan. Casia image tampering detection evaluation database. In *2013 IEEE China summit and international conference on signal and information processing*, pages 422–426. IEEE, 2013. [7](#), [8](#)
- [8] Pasquale Ferrara, Tiziano Bianchi, Alessia De Rosa, and Alessandro Piva. Image forgery localization via fine-grained analysis of cfa artifacts. *IEEE Transactions on Information Forensics and Security*, 7(5):1566–1577, 2012. [3](#), [6](#)
- [9] Haiying Guan, Mark Kozak, Eric Robertson, Yooyoung Lee, Amy N Yates, Andrew Delgado, Daniel Zhou, Timothee Kheykhah, Jeff Smith, and Jonathan Fiscus. Mfc datasets: Large-scale benchmark datasets for media forensic challenge evaluation. In *2019 IEEE Winter Applications of Computer Vision Workshops (WACVW)*, pages 63–72. IEEE, 2019. [7](#)
- [10] Yu-Feng Hsu and Shih-Fu Chang. Detecting image splicing using geometry invariants and camera characteristics consistency. In *2006 IEEE international conference on multimedia and expo*, pages 549–552. IEEE, 2006. [7](#)
- [11] Edward J Hu, Yelong Shen, Phillip Wallis, Zeyuan Allen-Zhu, Yuanzhi Li, Shean Wang, Lu Wang, Weizhu Chen, et al. Lora: Low-rank adaptation of large language models. *ICLR*, 1(2):3, 2022. [7](#)
- [12] Megi Isallari and Islem Rekik. Gsr-net: Graph super-resolution network for predicting high-resolution from low-resolution functional brain connectomes. In *International Workshop on Machine Learning in Medical Imaging*, pages 139–149. Springer, 2020. [1](#), [6](#)
- [13] VijayaKumar Kadha, Sambit Bakshi, and Santos Kumar Das. Unravelling digital forgeries: A systematic survey on image manipulation detection and localization. *ACM Computing Surveys*, 57(12):1–36, 2025. [3](#)
- [14] Chenqi Kong, Anwei Luo, Shiqi Wang, Haoliang Li, Anderson Rocha, and Alex C Kot. Pixel-inconsistency modeling for image manipulation localization. *IEEE Transactions on Pattern Analysis and Machine Intelligence*, 2025. [3](#)
- [15] Myung-Joon Kwon, In-Jae Yu, Seung-Hun Nam, and Heung-Kyu Lee. Cat-net: Compression artifact tracing network for detection and localization of image splicing. In *Proceedings of the IEEE/CVF winter conference on applications of computer vision*, pages 375–384, 2021. [1](#), [6](#)
- [16] Jiafeng Li, Ying Wen, and Lianghua He. M<sup>2</sup>rl-net: Multi-view and multi-level relation learning network for weakly-supervised image forgery detection. In *Proceedings of the AAAI Conference on Artificial Intelligence*, pages 4743–4751, 2025. [2](#), [3](#), [6](#), [8](#)

[17] Xuntao Liu, Yuzhou Yang, Qichao Ying, Zhenxing Qian, Xinpeng Zhang, and Sheng Li. Prompt-iml: Image manipulation localization with pre-trained foundation models through prompt tuning. *arXiv preprint arXiv:2401.00653*, 2024. 1

[18] Ilya Loshchilov and Frank Hutter. Decoupled weight decay regularization. *arXiv preprint arXiv:1711.05101*, 2017. 7

[19] Xiaochen Ma, Bo Du, Zhuohang Jiang, Ahmed Y Al Hammadi, and Jizhe Zhou. Iml-vit: Benchmarking image manipulation localization by vision transformer. *arXiv preprint arXiv:2307.14863*, 2023. 8

[20] Laurens van der Maaten and Geoffrey Hinton. Visualizing data using t-sne. *Journal of machine learning research*, 9 (Nov):2579–2605, 2008. 8

[21] Babak Mahdian and Stanislav Saic. Using noise inconsistencies for blind image forensics. *Image and vision computing*, 27(10):1497–1503, 2009. 3, 6

[22] Changtao Miao, Zichang Tan, Qi Chu, Nenghai Yu, and Guodong Guo. Hierarchical frequency-assisted interactive networks for face manipulation detection. *IEEE Transactions on Information Forensics and Security*, 17:3008–3021, 2022. 1

[23] Adam Novozamsky, Babak Mahdian, and Stanislav Saic. Imd2020: A large-scale annotated dataset tailored for detecting manipulated images. In *Proceedings of the IEEE/CVF winter conference on applications of computer vision workshops*, pages 71–80, 2020. 2, 3, 7, 8

[24] Deepak Pathak, Evan Shelhamer, Jonathan Long, and Trevor Darrell. Fully convolutional multi-class multiple instance learning. *arXiv preprint arXiv:1412.7144*, 2014. 2, 6

[25] Alec Radford, Jong Wook Kim, Chris Hallacy, Aditya Ramesh, Gabriel Goh, Sandhini Agarwal, Girish Sastry, Amanda Askell, Pamela Mishkin, Jack Clark, et al. Learning transferable visual models from natural language supervision. In *International conference on machine learning*, pages 8748–8763. PMLR, 2021. 2, 3, 5, 7

[26] Yuan Rao and Jiangqun Ni. A deep learning approach to detection of splicing and copy-move forgeries in images. In *2016 IEEE international workshop on information forensics and security (WIFS)*, pages 1–6. IEEE, 2016. 2

[27] Yongming Rao, Wenliang Zhao, Guangyi Chen, Yansong Tang, Zheng Zhu, Guan Huang, Jie Zhou, and Jiwen Lu. Denseclip: Language-guided dense prediction with context-aware prompting. In *Proceedings of the IEEE/CVF conference on computer vision and pattern recognition*, pages 18082–18091, 2022. 3

[28] Dianmo Sheng, Dongdong Chen, Zhentao Tan, Qiankun Liu, Qi Chu, Tao Gong, Bin Liu, Jing Han, Wenbin Tu, Shengwei Xu, et al. Unicl-sam: Uncertainty-driven in-context segmentation with part prototype discovery. In *Proceedings of the Computer Vision and Pattern Recognition Conference*, pages 20201–20211, 2025. 1

[29] Lei Su, Xiaochen Ma, Xuekang Zhu, Chaoqun Niu, Zeyu Lei, and Ji-Zhe Zhou. Can we get rid of handcrafted feature extractors? sparsevit: Nonsemantics-centered, parameter-efficient image manipulation localization through sparse-coding transformer. In *Proceedings of the AAAI Conference on Artificial Intelligence*, pages 7024–7032, 2025. 2

[30] Gregory K Wallace. The jpeg still picture compression standard. *Communications of the ACM*, 34(4):30–44, 1991. 8

[31] Haichou Wang, Hang Cheng, Yun Chen, Yongliang Xu, and Meiqing Wang. Image manipulation localization via semantic-guided feature enhancement and deep multi-scale edge supervision. *Neurocomputing*, page 130255, 2025. 3

[32] Junke Wang, Zuxuan Wu, Jingjing Chen, Xintong Han, Abhinav Shrivastava, Ser-Nam Lim, and Yu-Gang Jiang. Objectformer for image manipulation detection and localization. In *Proceedings of the IEEE/CVF conference on computer vision and pattern recognition*, pages 2364–2373, 2022. 3

[33] Xinghao Wang, Tao Gong, Qi Chu, Bin Liu, and Nenghai Yu. Context-aware weakly supervised image manipulation localization with sam refinement. *IEEE Signal Processing Letters*, 32:3047–3051, 2025. 2

[34] Bihai Wen, Ye Zhu, Ramanathan Subramanian, Tian-Tsong Ng, Xuanjing Shen, and Stefan Winkler. Coverage—a novel database for copy-move forgery detection. In *2016 IEEE international conference on image processing (ICIP)*, pages 161–165. IEEE, 2016. 7

[35] Yue Wu, Wael AbdAlmageed, and Premkumar Natarajan. Mantra-net: Manipulation tracing network for detection and localization of image forgeries with anomalous features. In *Proceedings of the IEEE/CVF conference on computer vision and pattern recognition*, pages 9543–9552, 2019. 1, 2, 6

[36] Chao Yang, Huizhou Li, Fangting Lin, Bin Jiang, and Hao Zhao. Constrained r-cnn: A general image manipulation detection model. *arXiv preprint arXiv:1911.08217*, 2019. 3

[37] Zeqin Yu, Jiangqun Ni, Jian Zhang, Haoyi Deng, and Yuzhen Lin. Reinforced multi-teacher knowledge distillation for efficient general image forgery detection and localization. In *Proceedings of the AAAI Conference on Artificial Intelligence*, pages 995–1003, 2025. 2

[38] Yuanhao Zhai, Tianyu Luan, David Doermann, and Junsong Yuan. Towards generic image manipulation detection with weakly-supervised self-consistency learning. In *Proceedings of the IEEE/CVF International Conference on Computer Vision*, pages 22390–22400, 2023. 2, 3, 6, 8

[39] Zhenfei Zhang, Ming-Ching Chang, and Xin Li. Training-free image manipulation localization using diffusion models. In *Proceedings of the AAAI Conference on Artificial Intelligence*, pages 10376–10384, 2025. 2

[40] Kaiyang Zhou, Jingkang Yang, Chen Change Loy, and Ziwei Liu. Learning to prompt for vision-language models. *International Journal of Computer Vision*, 130(9):2337–2348, 2022. 3

[41] Kaiyang Zhou, Jingkang Yang, Chen Change Loy, and Ziwei Liu. Conditional prompt learning for vision-language models. In *Proceedings of the IEEE/CVF conference on computer vision and pattern recognition*, pages 16816–16825, 2022. 3

[42] Peng Zhou, Bor-Chun Chen, Xintong Han, Mahyar Najibi, Abhinav Shrivastava, Ser-Nam Lim, and Larry Davis. Generate, segment, and refine: Towards generic manipulation segmentation. In *Proceedings of the AAAI conference on artificial intelligence*, pages 13058–13065, 2020. 3

[43] Yang Zhou, Hongxia Wang, Qiang Zeng, Rui Zhang, and Si-  
jiang Meng. Exploring weakly-supervised image manipula-  
tion localization with tampering edge-based class activation  
map. *Expert Systems with Applications*, 249:123501, 2024.  
[2](#)

[44] Zhangchen Zhu, Jiafeng Li, and Ying Wen. Self-  
optimization training for weakly supervised image manip-  
ulation localization. In *ICASSP 2025-2025 IEEE Interna-  
tional Conference on Acoustics, Speech and Signal Process-  
ing (ICASSP)*, pages 1–5. IEEE, 2025. [2](#), [3](#), [6](#), [8](#)